Journal of Power Sources 195 (2010) 5806–5809

Contents lists available at ScienceDirect

Journal of Power Sources

journal homepage: www.elsevier.com/locate/jpowsour

Short communication

Improvement of the performance of dye-sensitized solar cells using Sn-doped ZnO nanoparticles

Ning Ye[a,b], Junjie Qi[a], Zi Qi[a], Xiaomei Zhang[a], Ya Yang[a], Jing Liu[c], Yue Zhang[a,b,*]

[a] State Key Laboratory for Advanced Metals and Materials, Department of Materials Physics, University of Science and Technology Beijing, 100083 Beijing, People's Republic of China
[b] Key Laboratory of New Energy Materials and Technologies, University of Science and Technology Beijing, Beijing 100083, People's Republic of China
[c] School of Materials and Metallurgy, Wuhan University of Science and Technology, Wuhan 430081, Hubei, People's Republic of China

ARTICLE INFO

Article history:
Received 10 November 2009
Received in revised form 3 March 2010
Accepted 8 March 2010
Available online 15 March 2010

Keywords:
Dye-sensitized solar cell
ZnO
Sn-doped
Compact layer

ABSTRACT

Sn-doped and undoped ZnO nanoparticles were synthesized by hydrothermal method and their performance as the photoanode of dye-sensitized solar cells (DSSCs) was investigated. Energy dispersive X-ray spectroscopy and X-ray diffraction showed that the Sn had been doped into the ZnO lattice. A red shift of photoluminescence spectra which was induced by Sn doping was observed. The photocurrent density–voltage curves of DSSCs indicated that the efficiency was increased by as high as 140% on bare-FTO substrate and 105% on ZnO compact layer/FTO substrate via Sn doping. Also the effect of the ZnO compact layer was discussed by both of Sn-doped or undoped DSSCs.

1. Introduction

As a potential substitute for conventional solar energy conversion devices, dye-sensitized solar cells (DSSCs) have attracted much attention for their low costs and convenient fabrication [1–3]. To date, nanocrystalline TiO_2 film is the most successful photoanode of DSSCs, but there are many defects in the TiO_2-based DSSCs. For example, there are high surface states [4] and high surface charge recombination rate [5] in TiO_2-based DSSCs, which account for their low efficiency. Therefore, other wide band-gap semiconductors, such as ZnO [6,7], SnO_2 [8,9] and Nb_2O_5 [10] have been researched to substitute for TiO_2 as the photoanode. Among these semiconductors, ZnO is the most promising alternative to TiO_2 as the photoanode of DSSCs in the future. Boschloo and co-workers research has showed that the lifetime of electrons in ZnO electrode is much longer than that in TiO_2 electrode, and use of ZnO as the photoanode can effectively reduce the recombination rate of the electrons [11]. Much research work focus on the quasi-one-dimensional nanostructure ZnO electrodes. DSSCs fabricated with ZnO nanowire arrays [12,13], nanotetrapods [14,15], nanorods [16], nanoflowers [17,18] and branched nanowire arrays [19] have been reported. However, to the best of our knowledge, the highest conversion efficiency of ZnO-based DSSCs is achieved by ZnO nanoparticles [7]. Though much work has been done on modifying ZnO by doping of metal ions, such as Sn [20], In [21], Sb [22] and so forth, DSSCs fabricated with nanostructured Sn-doped ZnO photoanode has not been reported. On the other hand, since there are much work concentrating on the compact layer of DSSCs, which can certainly reduce the recombination of electrons [23–27], there is a question on how a ZnO compact layer impacts on the performance of Sn-doped ZnO-based DSSCs.

In the present work, we synthesized undoped and Sn-doped ZnO nanoparticles by hydrothermal method, then coated them onto bare-FTO substrate and ZnO compact layer/FTO substrate respectively. The characterization of these DSSCs show that the performance of ZnO-based DSSCs has been remarkably enhanced by Sn doping.

2. Experimental details

2.1. Synthesis and characterization of Sn-doped ZnO nanoparticles

Sn-doped ZnO nanomaterials were synthesized by hydrothermal method using zinc chloride, tin tetrachloride, polyethylene glycol 400 and sodium hydroxide. $ZnCl_2$ and $SnCl_4$ with a certain mole ratio (Sn/Zn = 1/100, 1/50, 1/20) were dissolved in 100 ml deionized water. Then 25 ml of polyethylene glycol 400 was added into the solution. The pH value of the solution was adjusted to 12 by adding 2 M NaOH into the solution while stirring (500 rpm) for 1 h. Then, the resultant mixture was transferred into an autoclave and heated at 160 °C for 5 h. The obtained precipitates were rinsed sev-

* Corresponding author. Tel.: +86 10 62334725; fax: +86 10 62332281.
E-mail address: yuezhang@ustb.edu.cn (Y. Zhang).

0378-7753/$ – see front matter © 2010 Elsevier B.V. All rights reserved.
doi:10.1016/j.jpowsour.2010.03.036

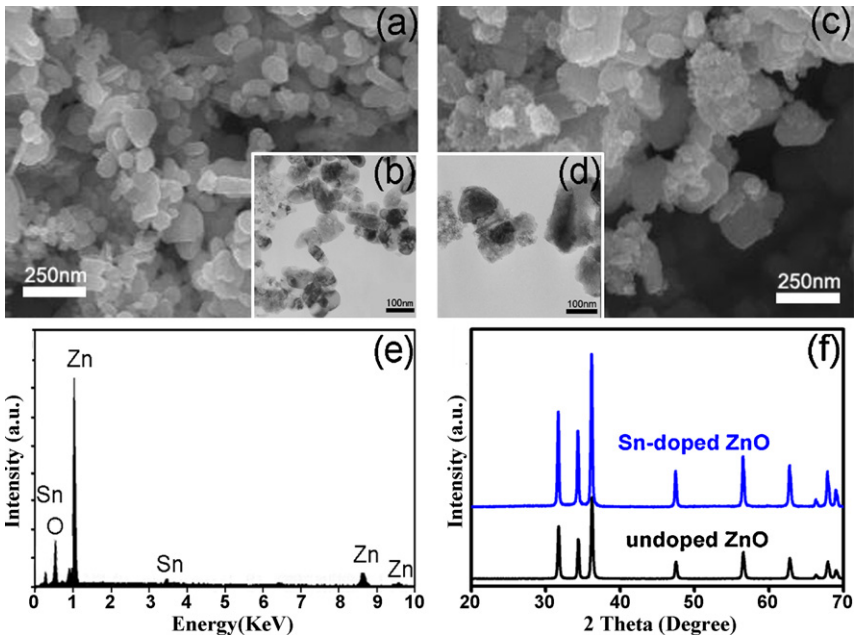

Fig. 1. (a) FE-SEM image of undoped ZnO nanoparticles. (b) TEM image of undoped ZnO nanoparticles. (c) FE-SEM image of Sn-doped ZnO nanoparticles. (d) TEM image of Sn-doped ZnO nanoparticles. (e) EDS of Sn-doped ZnO powders. (f) XRD of undoped and 5.5 wt% Sn-doped ZnO.

eral times by deionized water and ethanol, and then dried at 70 °C for 24 h and calcined at 400 °C for 1 h. The undoped ZnO powders were synthesized in the same condition without adding the tin salt.

The structure of as-synthesized powders was examined using field emission scanning electron microscopy (FE-SEM, SUPRA^{TM55}) and transmitting electron microscopy (TEM, JEOL, JEM-1200EX). X-ray diffraction (XRD, Rigaku DMAX-RB) and energy dispersive X-ray spectroscopy (EDS) were used to analyze the phase and the content of dopant. The photoluminescence (PL) measurement was performed using a HR800 UV–vis Raman spectrometer (Horiba/Jobin–Yvon).

2.2. Solar cells preparation and characterization

The electrodes were prepared on bare FTOs (14 Ω/□, Nippon Sheet Glass, Japan) and ZnO compact layer/FTO respectively by doctor blade method [2]. To form the ZnO compact layer, the solution of zinc acetate dissolved in ethylene glycol monomethyl ether was spin-coated onto the FTO and then the substrate was calcined at 350 °C for 1 h. The paste was prepared by mixing the synthesized powders, ethyl cellulose, terpineol, Triton-X and polyethylene glycol 20000. Then the DSSCs electrodes were prepared by squeezing the paste onto the substrates using plastic tapes with thickness of 100 μm. The as-prepared electrode was annealed for 30 min at 450 °C in air and then cooled. The as-annealed electrodes were immersed into a 0.2 mM N719 (ruthenium (2,2′-bipyridyl-4,4′-dicarboxilate)$_2$(NCS)$_2$, Dyesol, Australia) ethanol solution for 90 min. Finally, the dye-absorbed electrodes were assembled with the prepared Pt counter electrodes to form a sandwich-type DSSCs using a sealing plastic (25 μm, SX-1170-25, Solaronix).

The current–voltage (*I–V*) characteristics of the DSSCs were recorded by an electrochemical interface instruments (Solartron SI 1287/SI 1260), with a solar simulator (Oriel, 91159A) served as the light source.

3. Experimental results and discussion

Fig. 1a–d shows the morphology of the synthesized powders. In the images, it is seen that both the undoped ZnO and Sn-doped ZnO powders have equal particles' size(∼100 nm). Furthermore, the surface of Sn-doped ZnO particles become rough, compared with the smooth surface of undoped ZnO nanoparticles, indicating that the Sn-doped ZnO powders have higher specific surface area than the undoped ones. Fig. 1e shows the typical EDS spectra from Sn-doped ZnO powders. The Sn contents are identified to be about 1.9 wt%, 2.5 wt%, 5.5 wt% respectively, corresponding to three different mixture ratio of 1/100, 1/50, 1/20. The XRD results also indicate that no second phase is detected in both undoped ZnO and Sn-doped ZnO powders in Fig. 1f. All the peaks of the XRD pattern are identified precisely to those of the ZnO wurtzite structure (a = 0.3249 nm and c = 0.52 nm, Joint Committee on Powder Diffraction Standards (JCPDS) card number 36-1451). The structure of the ZnO powders did not change much due to the doping of Sn. Therefore, the Sn^{4+} ions must have been doped into the ZnO lattice successfully by hydrothermal reaction.

The room-temperature PL spectra recorded from undoped ZnO and 5.5 wt% Sn-doped ZnO powders was shown in Fig. 2. The light source is a He–Cd ion laser (325 nm). The PL spectra from Sn-doped ZnO powders reveal a red shift comparing with those from undoped powders. Furthermore, the undoped ZnO powders exhibited the ultraviolet (UV) emission band at 3.22 eV while the UV emission band of Sn-doped ZnO is located at 3.18 eV. In the PL spectra from

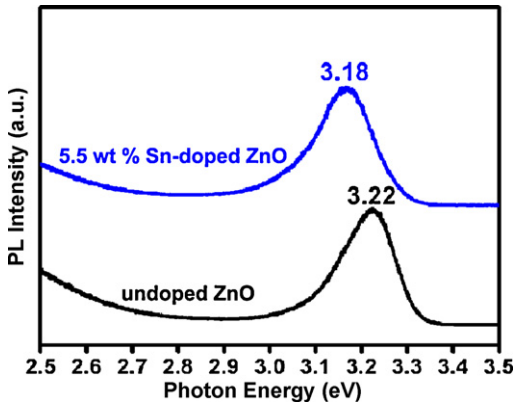

Fig. 2. PL spectra from undoped ZnO and 5.5 wt% Sn-doped ZnO.

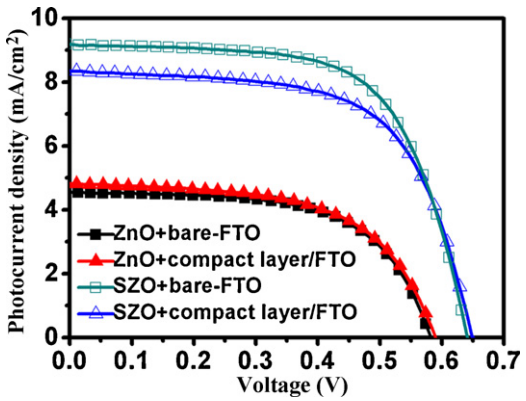

Fig. 3. the *J*–*V* curves of DSSCs with and without ZnO compact layer with undoped and 5.5 wt% Sn-doped ZnO porous film at AM 1.5 irradiation of 100 mW cm^{-2}. (In the graph, SZO represents Sn-doped ZnO.)

ZnO, the UV emission band is also known as the near band edge peak, which is attributed to the recombination of free excitons of ZnO [28,29]. The red shift of UV emission caused by Sn doping could be explained by the narrowing of energy band-gap.

Fig. 3 presents the photocurrent density–voltage (*J*–*V*) curves of DSSCs with and without ZnO compact layer with ~12 μm undoped and 5.5 wt% Sn-doped ZnO porous film at AM 1.5 irradiation of 100 mW cm^{-2}. Table 1 summarizes their photovoltaic properties. The effect of different Sn content on the performance of DSSCs were also investigated. The efficiencies of the DSSCs were improved with the increasing of Sn doping. The photo-to-current conversion efficiency values are 1.62%, 2.08%, 2.43% and 3.79% respectively corresponding to different photoanode of undoped, 1.9 wt%, 2.5 wt% and 5.5 wt% Sn-doped ZnO without compact layer. It is noticeable that Sn doping increases both J_{sc} and V_{oc} of ZnO-based DSSCs significantly regardless of type of the substrates used (bare-FTO or on ZnO compact layer/FTO). For the ZnO-based DSSCs with bare-FTO substrate, the J_{sc} increases by 102% after 5.5 wt% Sn doping. On the other hand, for the DSSCs with ZnO compact layer/FTO substrate, the J_{sc} of 5.5 wt% Sn-doped ZnO-based DSSCs increases by 73% compared with that of undoped ones. This increase can be attributed to morphology change and increase of the charge carriers density which are caused by doping. As is known, Sn-doped ZnO is a kind of N-type doping, which leads to the increase of the charge carriers density and the rising of Fermi energy levels. The electrons transport capacity of ZnO is enhanced due to the increase of charge carriers density by the doping. Charge carrier density increase results in the increase of J_{sc}. As discussed above for Fig. 1, the Sn-doped ZnO has the rougher surface than the undoped ZnO, indicating that the former one has higher specific surface area to absorb more dye molecules. It could also result in the enhancement of J_{sc}. On the other hand, the enhancement of the V_{oc} by doing can be explained by the following two reasons. First, the electron concentration at V_{oc} increase with the improvement of the electrons transport capacity by Sn doping. Secondly, Sn doping, the N-type doping, makes the Fermi energy levels rise, which will result in the increase of V_{oc} since the V_{oc} represents the difference between E_F and $E_{electrolyte}$ [30]. Ultimately, via the Sn doping, the photo-to-current conversion efficiency of ZnO-based DSSCs on the bare-FTO substrate is increased by as high as 140% while that of ZnO-based DSSCs on the ZnO compact layer/FTO substrate is increased by 105%.

Table 1
Photovoltaic properties of DSSCs with active area of 0.2 cm^2 (AM 1.5G, 100 mW cm^{-2}).

Sample	J_{sc} (mA cm^{-2})	V_{oc} (V)	ff	η (%)
Undoped ZnO + bare FTO	4.55	0.581	0.62	1.62
Undoped ZnO + FTO with ZnO compact layer	4.82	0.590	0.59	1.66
5.5 wt% Sn-doped ZnO + bare FTO	9.18	0.641	0.65	3.79
5.5 wt% Sn-doped ZnO + FTO with ZnO compact layer	8.36	0.648	0.64	3.40

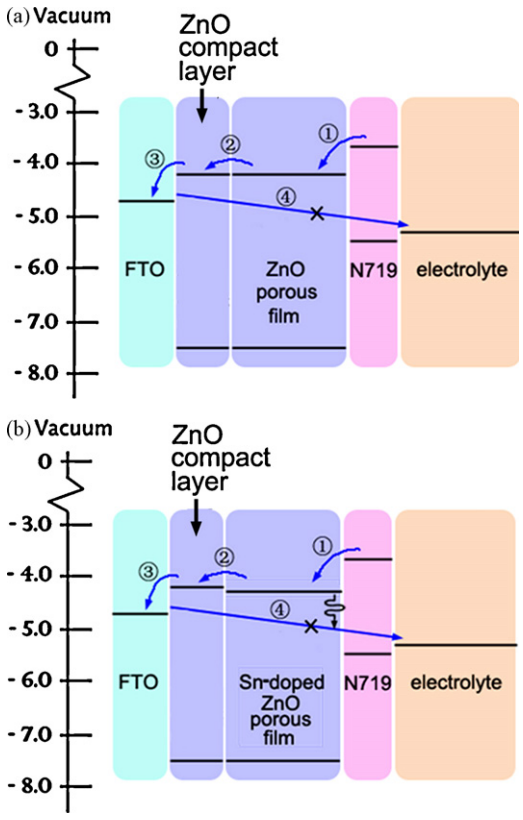

Fig. 4. Illustrations of the band diagrams (a) for the DSSCs with undoped ZnO on ZnO compact layer/FTO substrate, (b) for the DSSCs with Sn-doped ZnO on ZnO compact layer/FTO substrate.

Furthermore, while the introduction of ZnO compact layer is observed to be beneficial to the efficiency of undoped ZnO-based DSSCs, it results in a decline in the efficiency of Sn-doped ZnO-based DSSCs. In the undoped ZnO-based DSSCs, introduction of the ZnO compact layer increases both the J_{sc} and the V_{oc} slightly. As illustrated in Fig. 4a, while the ZnO compact layer prevents the FTO from contacting the electrolyte, it suppresses the transfer of back electron from FTO to electrolyte (blocking layer effect) by cutting off the process ④. This result is consistent with the previous reports [23,27], in which the compact layer acts as a blocking layer. However, for the Sn-doped ZnO-based DSSCs, the introduction of ZnO compact layer has little impacts on the V_{oc}, but leads to a definite decrease in the J_{sc} and the efficiency. This reduction of the J_{sc} which accounts for the decrease of the efficiency might be ascribed to the reason elucidated as follows. As discussed above, induced by doping, the energy band-gap of Sn-doped ZnO becomes a little narrower than that of undoped ZnO. Therefore, the conduction band of Sn-doped ZnO porous film will become a little lower than that of ZnO compact layer which is shown in Fig. 4b. That indicates the electrons in the conduction band of Sn-doped ZnO, which come from the lowest unoccupied molecular orbital (LUMO) of the dye, could not completely inject into the conduction band of ZnO compact layer by the process ② even under the theoretical conditions. In other words, when the electrons transfer from the conduction band

of Sn-doped ZnO to that of ZnO compact layer, the electrons whose energy are between the conduction band of Sn-doped ZnO and the conduction band of ZnO compact layer will be recombined by redox instead of forming the photocurrent. Consequently, in Sn-doped ZnO-based DSSCs, though the ZnO compact layer still suppresses the transfer of back electron from FTO to electrolyte, this reduction of recombination cannot compensate for the electrons recombination when transferring from the Sn-doped ZnO porous film to the ZnO compact layer. This is probable the reason why the J_{sc} of Sn-doped ZnO-based DSSCs decreases after the introduction of the ZnO compact layer.

4. Conclusions

In summary, the efficiency of DSSCs fabricated with Sn-doped ZnO is observed to be remarkably higher than that of DSSCs with undoped ZnO. This enhancement is due to the co-action of morphology change, increase of the charge carriers density and heightening of Fermi energy levels, which is induced by Sn doping. In addition, we observe that the introduction of ZnO compact layer increases the efficiency of undoped ZnO-based DSSCs by blocking layer effect, but decreases the efficiency of Sn-doped ZnO-based DSSCs, which might be ascribed to the electron recombination when electrons transferred from porous film to compact film.

Acknowledgements

This work was supported by the Major Project of International Cooperation Exchanges (No. 50620120439, 2006DFB51000), the National Basic Research Program of China (No. 2007CB936201) and the National Natural Science Foundation of China (Nos. 10876001 and 50872008).

References

[1] B. O'Regan, M. Grätzel, Nature 353 (1991) 737.
[2] M.K. Nazeeruddin, A. Kay, I. Rodocio, R. Humphry-Baker, E. Muller, P. Liska, N. Vlachopoulos, M. Grätzel, J. Am. Chem. Soc. 115 (1993) 6382.
[3] M. Grätzel, Nature 414 (2001) 338.
[4] J. van de Lagemaat, A.J. Frank, J. Phys. Chem. B 104 (2000) 4292.
[5] S. Nakade, Y. Saito, W. Kubo, T. Kitamura, Y. Wada, S. Yanagida, J. Phys. Chem. B 107 (2003) 8607.
[6] H. Rensmo, K. Keis, H. Lindström, S. Södergren, A. Solbrand, A. Hagfeldt, S.E. Lindquist, L.N. Wang, M. Muhammed, J. Phys. Chem. B 101 (1997) 2598.
[7] M. Saito, S. Fujihara, Energy Environ. Sci. 1 (2008) 280.
[8] R. Dabestani, A.J. Bard, A. Campion, M.A. Fox, T.E. Mallouk, S.E. Webber, J.M. White, J. Phys. Chem. 92 (1988) 1872.
[9] S. Gubbala, V. Chakrapani, V. Kumar, M.K. Sunkara, Adv. Funct. Mater. 18 (2008) 2411.
[10] F. Lenzmann, J. Krueger, S. Burnside, K. Brooks, M. Grätzel, D. Gal, S. Rühle, D. Cahen, J. Phys. Chem. B 105 (2001) 6347.
[11] M. Quintana, T. Edvinsson, A. Hagfeldt, G. Boschloo, J. Phys. Chem. C 111 (2007) 1035.
[12] M. Law, L. Greene, J.C. Johnson, Nat. Mater. 4 (2005) 455.
[13] J.B. Baxter, E.S. Aydil, Appl. Phys. Lett. 86 (2005) 053114.
[14] Y.F. Hsu, Y.Y. Xi, C.T. Yip, A.B. Djurišić, W.K. Chan, J. Appl. Phys. 103 (2008) 083114.
[15] W. Chen, H. Zhang, I.M. Hsing, S. Yang, Electrochem. Commun. 11 (2009) 1057.
[16] Y.F. Hsu, Y.Y. Xi, A.B. Djurišić, W.K. Chan, Appl. Phys. Lett. 92 (2008) 133507.
[17] C.Y. Jiang, X.W. Sun, G.Q. Lo, D.L. Kwong, J.X. Wang, Appl. Phys. Lett. 90 (2007) 263501.
[18] V. Dhas, S. Muduli, W. Lee, S.H. Han, S. Ogale, Appl. Phys. Lett. 93 (2008) 243108.
[19] H.M. Cheng, W.H. Chiu, C.H. Lee, S.Y. Tsai, W.F. Hsieh, J. Phys. Chem. C 112 (2008) 16359.
[20] S.Y. Bae, C.W. Na, J.H. Kang, J. Park, J. Phys. Chem. B 109 (2005) 2526.
[21] J. Qi, Y. Zhang, Y. Huang, Q. Liao, J. Liu, Appl. Phys. Lett. 89 (2006) 252115.
[22] Y. Yang, J. Qi, Q. Liao, Y. Zhang, L. Tang, Z. Qin, J. Phys. Chem. C 112 (2008) 17916.
[23] U. Bach, D. Lupo, P. Compte, J.E. Moser, F. Weissörtel, J. Salbeck, H. Spreitzer, M. Grätzel, Nature 395 (1998) 583.
[24] H.J. Snaith, M. Grätzel, Adv. Mater. 18 (2006) 1910.
[25] A. Burke, S. Ito, H. Snaith, U. Bach, J. Kwiatkowski, M. Grätzel, Nano Lett. 8 (2008) 977.
[26] J. Xia, N. Masaki, K. Jiang, S. Yanagida, J. Phys. Chem. C 111 (2007) 8092.
[27] S. Lee, J.H. Noh, H.S. Han, D.K. Yim, D.H. Kim, J.K. Lee, J.Y. Kim, H.S. Jung, K.S. Hong, J. Phys. Chem. C 113 (2009) 6878.
[28] D.C. Reynolds, D.C. Look, B. Jogai, C.W. Litton, T.C. Collins, W.C. Harsch, G. Cantwell, Phys. Rev. B 57 (1998) 12151.
[29] T. Matsumoto, H. Kato, K. Miyamoto, M. Sano, E.A. Zhukov, T. Yao, Appl. Phys. Lett. 81 (2002) 1231.
[30] Y. Diamant, S.G. Chen, O. Melamed, A. Zaban, J. Phys. Chem. B 107 (2003) 1977.